Grasping and Manipulation of a Micro-particle using Multiple Optical Traps

Chien Chern Cheah, Quang Minh Ta, Reza Haghighi

School of Electrical and Electronic Engineering, Nanyang Technological University, Singapore

Abstract

In existing control techniques for optical tweezers, a target particle is directly trapped and manipulated by a single laser beam. However, a typical force generated by an optical trap is extremely small (on the order of pico-newtons) and thus it is not sufficient to manipulate a large cell or object. Besides, the feasibility of optical manipulation also depends on the physical properties of the specimen. An opaque object or object with the same refractive index as the fluid media may not be trapped directly by the laser beam. Therefore, current control techniques for optical tweezers cannot be utilized to manipulate various types of cells or objects, including untrappable or large ones. In this paper, robotic control techniques are developed for optical tweezers to achieve grasping and manipulation of a microscopic particle, which is beyond the capability of a single optical trap. First, multiple laser beams are generated, and each laser beam is utilized to trap and drive one grasping particle to form a desired shape around the target particle. A grasping formation of trapped particles is thus generated to hold the target particle. Then the target particle is manipulated to a desired position by controlling the motorized stage. The proposed control strategy is particularly suitable for manipulation of large particles, or even untrappable cells or objects. Rigorous mathematical formulations have been developed to analyze the control system for grasping and manipulation of the microscopic particle. Experimental results are presented to illustrate the performance of the proposed grasping and manipulation techniques.

Key words: microsystems: nano- and micro-technologies, robotics technology, optical manipulation, motion control, grasping

1 Introduction

Micromanipulation is currently of increasing interest due to its wide range of applications in biology science and micro-system technology. Techniques that have been utilized for micromanipulation include atomic force microscopy [1], mechanical micromanipulator [2, 3], magnetic tweezers [4, 5], electromagnetic tweezers [6], and optical tweezers [7]. Among these techniques, optical tweezers has received considerable attention because of its ability to manipulate microscopic objects precisely using highly focused laser beams.

The pioneer work in this field was conducted by Askin [8] in early 1970s. It was then demonstrated that a focused laser beam is able to tweeze and manipulate various types of objects such as dielectric micro-particles, viruses, bacteria, atoms, and molecules [9, 10]. Optical tweezers have been frequently utilized for manipulation of biological cells in recent years. Applications include cell separation [11], study of structure and mechanical properties of DNA [12], and analysis of human red blood cells [13].

In many applications, it is required to generate and manipulate multiple traps simultaneously. Techniques that have been developed to generate multiple traps include acousto-optic deflectors (AODs) [14], laser scanning method [15, 16], and holographic optical tweezers (HOT) [17]. The capability to generate and manipulate multiple traps independently at the same time has contributed extensively to the popularity of optical tweezing. Hence it has been utilized in many applications such as manipulation and assembling complex structures [18], multiple particle sorting [19], and indirect cell manipulation [20, 21].

Demand for precise, efficient and reliable manipulation of optical trapping has led to the development of automatic manipulation methods. Several control techniques have been proposed to improve the efficiency and performance of micromanipulation. A simple control scheme developed for manipulation of micro-scopic ob-

⋆ A preliminary result of this paper was presented in IEEE International Conference on Robotics and Automation ICRA, USA, 2015. Corresponding author Q. M. Ta. Tel. +65-9094-7353.

Email addresses: quangminh001@e.ntu.edu.sg (Quang Minh Ta), reza0007@e.ntu.edu.sg (Reza Haghighi).

jects was presented in [22]. Hu and Sun [23] proposed a PID controller and a synchronization control technique for transportation of biological cells. Ranaweeraz *et al.* [24] discussed the performance of linear and nonlinear controllers for manipulation of spherical particles. An automated technique for trapping and manipulation of non-spherical objects based on computer vision techniques was presented in [25]. Li and Cheah [26] employed a dynamic region control technique to allow flexibility in optical manipulation tasks. The integrated trapping and control technique for cell manipulation with the consideration of both cell and manipulator dynamics for closed-loop control was developed in [27]. Yan *et al.* [28] investigated the dynamic optical trapping problem of micro-particles under random perturbations and developed a controller with a velocity constraint based on the analysis. Besides, several control techniques have been proposed for automated manipulation of multiple particles. Chen and Sun [29] utilized holographic optical tweezers to drive every pair of micro-particles into an assigned array. In [30], a flocking controller has been developed to move all trapped micro-particles into a desired region without collision. Reza and Cheah [31] proposed a control methodology for dynamic manipulation of multiple groups of cells.

As the typical trapping force of a laser beam is very small, the target particle may escape from the trap during the manipulation process. In order to assure the completion of the manipulation task, it is usually required to increase the trapping stiffness by increasing the laser power. However, the use of a high intensity laser beam to directly trap and manipulate the biological cell may cause photo-damage or even lead to the death of the cell. To avoid cell photo-damage, Chowdhury *et al.* [21] proposed an indirect manipulation technique for cells using silica beads. The A* path planning algorithm was employed to generate a collision-free path for the system composed of the target cell and micro-beads. However, the work in [21] considered only the path planning problem while the dynamic interactions between the target cell and micro-beads, control law and stability analysis have not been taken into account for automated manipulation of cells.

In addition, optical trapping is also dependent on the physical properties of cells or objects. Current control techniques for optical tweezers cannot be utilized to manipulate various types of microscopic particles, such as large particles, laser-sensitive biological cells, or particles that cannot be trapped by the laser beam such as opaque objects. In this paper, robotic control techniques are proposed to achieve grasping and manipulation of a microscopic particle using multiple optical traps. Besides, rotation of particles, which cannot be performed by using single optical trap, is also achieved. In this control strategy, multiple laser beams are first generated, and each laser beam is utilized to trap and automatically drive an identical trappable micro-particle to form a desired shape around the target particle. A grasping formation of trapped micro-particles is thus generated to hold the target particle. The target particle is then manipulated to a desired position by using the motorized stage. Finally, the target particle can be released from the grasping formation. The manipulation control law is developed with the consideration of the dynamic interaction between the target particle and grasping particles. Moreover, the dynamics of the motorized stage is considered so that a complete control problem can be formulated and solved. The proposed control strategy is particularly desirable for manipulation of laser-sensitive biological cells, large particles, or even particles that are not trappable by optical tweezers. The main contribution of this paper is the formulation and solution of a robotic control problem to achieve a complete grasping and manipulation task in the microworld, which is beyond the capability of single optical trapping. The stability of the system is analyzed by using Lyapunov-like analysis, and experimental results are presented to demonstrate the performance of the proposed controllers. A preliminary version of this paper was accepted for presentation in [32]. The result in [32] required a time-consuming manual operation to allocate and adjust the grasping particles around the target particle to hold it. This paper presents the extended version which includes a grasping technique to achieve a complete grasping and manipulation task of a microscopic particle. New experimental results on grasping and manipulation of the micro-particle are also presented.

2 Background on optical tweezers and problem statement

Optical tweezers are utilized to trap and manipulate microscopic objects using highly focused laser beams. When light travels through the microscale object, the transfer of momentum from photons to the object results in a trapping force that keeps the object near the center of the laser beam. A typical optical-tweezer system is shown in Fig. 1. The laser beam is expanded by a beam expander, reflected on dichroic mirror, then introduced into the inverted microscope to create a trap at the sample plane.

In order to achieve multiplexed optical tweezers, acousto-optic deflectors (AODs) are commonly used for generating multiple traps simultaneously. An acousto-optic deflector consists of a crystal whose refractive index is determined by variations of sound wave frequency. Hence, varying the frequency of the sound wave results in different deflection angles of the diffracted beam.

In this paper, robotic control techniques are developed to achieve grasping and manipulation of a microscopic particle, which resolves problems of existing control techniques of optical tweezers using single optical trapping.

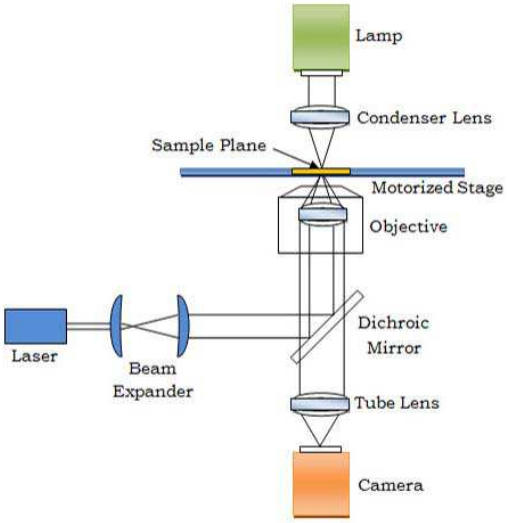

Fig. 1. A schematic of the optical tweezers system.

In this control strategy, a region control technique is utilized to first generate a grasping formation around the target particle to hold it, and the target particle is then manipulated to a desired position by controlling the motorized stage. An illustration of the control strategy is shown in Fig. 2.

The control strategy is described as follows: First, n laser beams are generated, and each laser beam is utilized to trap an identical trappable micro-particle such as a micro-bead. Using a region control technique, n trapped grasping particles are automatically moved to a desired shape or region around the target particle, and at the same time, kept a defined minimum distance between each other. The region is then scaled down to form a grasping formation around the target particle to hold it in a static position. An illustration of the grasping formation is shown in Fig. 3. After the target particle is held by trapped micro-particles, the laser beams will be kept fixed in the FOV, and the target particle is thus suspended in the medium. Then the target particle is manipulated to a desired position by the motorized stage which thus acts as a robotic manipulator.

3 Grasping formation control of trapped particles using a region control technique

In this section, a region control technique [33] is utilized to develop a robotic grasping strategy for the microscopic particle. By using the proposed strategy, the target particle can also be rotated. First, the laser beams are employed to trap and then move the grasping particles to form a desired shape specified by a desired region, and at the same time, keep the minimum distance between them. In order to hold the target particle in 2-D space, it is required to have at least three trapped micro-particles to form three contact points [34].

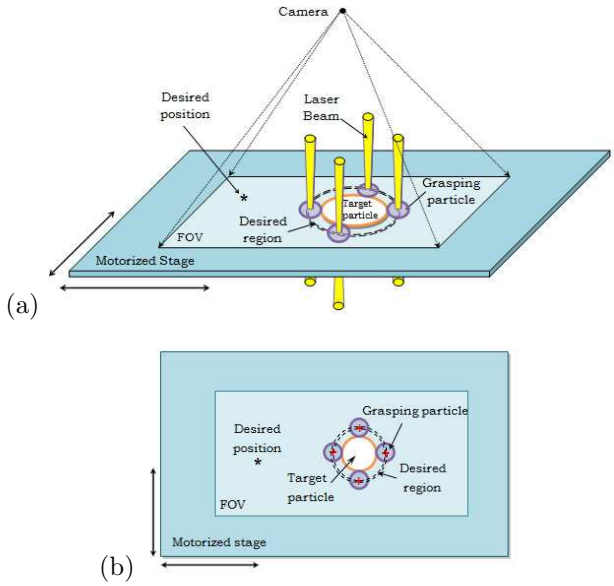

Fig. 2. An illustration of the control strategy. A grasping formation of four optically trapped particles is generated to first hold the target particle. The target particle is thus suspended in the medium. Then moving the motorized stage while fixing the laser beams in the field of view (FOV) of the camera varies the relative position between the target particle and the stage. (a) a 3-D view. The FOV is fixed while the motorized stage moves in 2-D space. (b) a 2-D view. The "+" denotes the laser beam position.

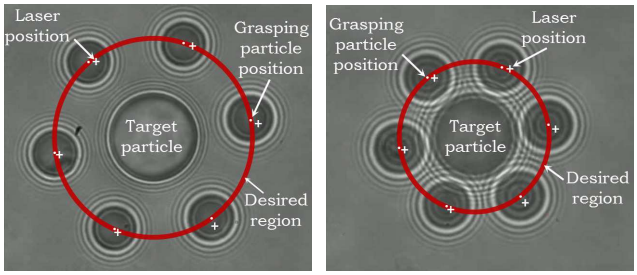

Fig. 3. An illustration of a grasping formation achieved by a time-varying region. First, six lasers are utilized to drive six grasping particles to the desired region centred around the target object while keeping the minimum distance between them. This region is then shrunk to hold the target object.

In this control problem, both the position of the target particle and the positions of the grasping particles are specified in the stage coordinate frame $\sum_S$ that is attached to the motorized stage and moving with the stage, and the positions of the laser beams are defined with respect to the reference frame $\sum_C$ that is fixed with the field of view (FOV) of the camera. The coordinate specification is illustrated in Fig. 4. The dynamics of the i^{th}

grasping particle is described as follows:

$$\underbrace{-\mathbf{B_b}\dot{\mathbf{y}}_\mathbf{i}}_{viscous force} \underbrace{+k\big((\mathbf{q_i}+\mathbf{z})-\mathbf{y_i}\big)}_{trapping force} = 0, \quad i = 1, 2, \ldots, n. \tag{1}$$

where $\mathbf{B_b} = diag\{b_{b1}, b_{b2}\} \in \mathbb{R}^{2x2}$ denotes the damping matrix which is diagonal and positive definite, and k represents the stiffness of the optical trap, and $\mathbf{y_i} = [y_{i1}, y_{i2}]^T \in \mathbb{R}^2$ is the position of the i^{th} grasping particle with respect to the stage coordinate frame $\sum_S$, $\mathbf{q_i}$ is the position of the i^{th} laser beam with respect to the reference frame $\sum_C$, and $\mathbf{z} = z_1, z_2]^T \in \mathbb{R}^2$ is the position of the origin of the reference frame $\sum_C$ with respect to the stage coordinate frame $\sum_S$. The first term in (1) is the viscous force due to the viscosity of the fluid medium. The trapping force of the laser beam is proportional to the small displacement between the position of the laser beam and the position of the grasping particle. As illustrated in Fig. 4, this displacement is represented by $\big((\mathbf{q_i}+\mathbf{z})-\mathbf{y_i}\big)$. In the grasping process, the motorized stage is kept fixed with respect to the FOV and hence $\mathbf{z}$ is constant, while $\mathbf{q_i}$ is varied by using acousto-optic deflectors. Note that in micromanipulation, the mass of the micro-particle can be ignored due to the dominance of drag force.

The desired shape of the grasping particles centred around the target particle is specified by the following desired region [26, 33]:

$$f(\Delta Y_i) = [f_1(\Delta Y_i), f_2(\Delta Y_i), \ldots, f_m(\Delta Y_i)]^T \leq 0, \tag{2}$$

where $\Delta Y_i = \mathbf{T}^{-1}(\mathbf{y_i} - \mathbf{x}) = \mathbf{T}^{-1}\Delta\mathbf{y_i}$. Note that the desired region is the intersection of all the objective functions. The position of the target particle with respect to the stage coordinate frame $\mathbf{x} = [x_1, x_2]^T \in \mathbb{R}^2$ is the reference point of the desired region, $\mathbf{T}$ is a time-varying transformation matrix which is differentiable and invertible, and $\mathbf{T}^{-1}$ is the inverse of the transformation matrix $\mathbf{T}$. The functions $f_l(\Delta Y_i)$, $l = 1, 2, ..., m$ are scalar

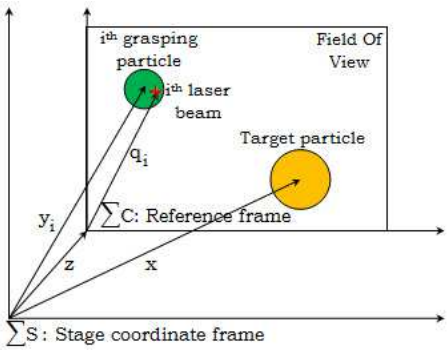

Fig. 4. The coordinates of the optical tweezers system. Stage coordinate frame $\sum_S$ attaches and moves with the motorized stage, while reference frame $\sum_C$ is fixed with the FOV of the camera.

functions with continuous partial derivatives, where m is the total number of objective functions.

Note that various desired regions or grasping formations can be formed by choosing appropriate objective functions. For example, the desired region in Fig. 5(a), which is the intersection of two concentric ellipses, can be formed by choosing the objective function as follows:

$$\begin{aligned} f_1(\Delta Y_i) &= 1 - \tfrac{\{\Delta Y_{i1}\}^2}{a_1^2} - \tfrac{\{\Delta Y_{i2}\}^2}{b_1^2} \leq 0 \\ f_2(\Delta Y_i) &= \tfrac{\{\Delta Y_{i1}\}^2}{a_2^2} + \tfrac{\{\Delta Y_{i2}\}^2}{b_2^2} - 1 \leq 0 \end{aligned} \tag{3}$$

where $\begin{pmatrix} \Delta Y_{i1} \\ \Delta Y_{i2} \end{pmatrix} = \mathbf{T}^{-1} \begin{pmatrix} y_{i1} - x_1 \\ y_{i2} - x_2 \end{pmatrix}$. a_1, a_2 and b_1, b_2 are the semi-major and semi-minor axes of the two ellipses, where $a_2 = a_1 + \delta_a$ and $b_2 = b_1 + \delta_b$ with positive parameter δ_a, δ_b. Note that when $a_1 = b_1 = R_1$ and $a_2 = b_2 = R_2$, the grasping formation becomes a ring, and when the transformation matrix $\mathbf{T}$ is equal to the identity matrix, i.e. $\mathbf{T} = \mathbf{I_2}$, the desired region is a static ring.

Note that the size and orientation of the desired region can be varied by the transformation mapping $\mathbf{T}$. An example of a rotational matrix $\mathbf{R}$ and a scaling matrix $\mathbf{S}$ in 2D is given by:

$$\mathbf{R} = \begin{bmatrix} \cos\phi(t) & \sin\phi(t) \\ -\sin\phi(t) & \cos\phi(t) \end{bmatrix}, \mathbf{S} = \begin{bmatrix} s_x(t) & 0 \\ 0 & s_y(t) \end{bmatrix}$$

respectively, where $\phi(t)$ is the angle of the rotation, $s_x(t)$ and $s_y(t)$ are scaling factors. By using either scaling or rotational matrix, or the combination of them, various grasping tasks can be performed. As illustrated in Fig. 5(b), by using the scaling transformation matrix $\mathbf{S}$, the desired region is thus scaled down to form the grasping formation that holds the target particle. Then the target particle is also rotated by rotating the grasping formation (Fig. 5(c)) using the rotational transformation matrix $\mathbf{R}$. Thus, a transformation matrix for both scaling and rotation is given as $\mathbf{T} = \mathbf{RS}$.

Another example is illustrated in Fig. 6 where the desired region of grasping particles is first rotated to an appropriate orientation with respect to the target particle. Then the region is scaled down to generate a grasping formation that holds the target particle.

A potential energy function of the global objective function (2) involving the i^{th} grasping particle is defined as:

$$P_i = \sum_{l=1}^{m} \frac{k_l}{\beta} [\max(0, f_l(\Delta Y_i)]^\beta, \tag{4}$$

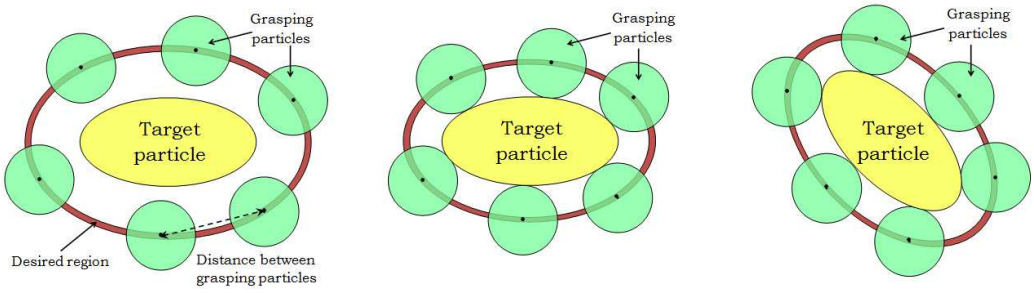

(a) (b) (c)

Fig. 5. An illustration of grasping and rotating of a target particle by using the time-varying region. The desired region is obtained by the intersections of 2 concentric ellipses. The transformation matrix is used to scale and rotate the desired region. The region is first scaled down to form a grasping formation that holds the target object (Fig. 5(b)). Then the target object is rotated by using a rotational transformation matrix. (Fig. 5(c))

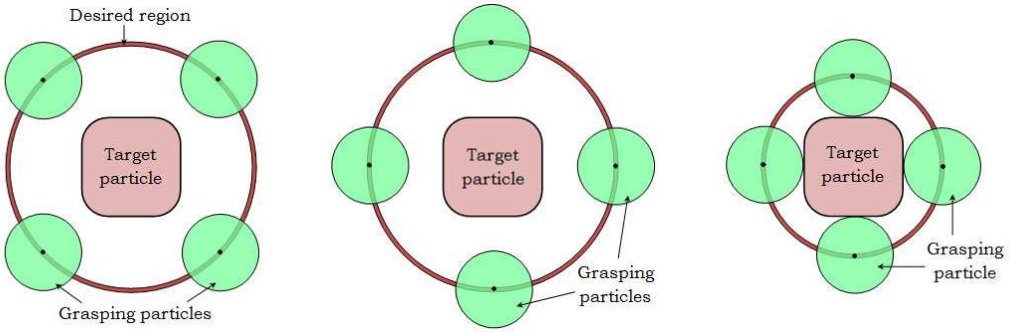

(a) (b) (c)

Fig. 6. Another illustration of using a transformed region to perform the grasping task. By using rotational transformation matrix $\mathbf{T} = \mathbf{R}$, the desired region (Fig. 6(a)) is first rotated to find stable grasping points. Then using scaling transformation matrix $\mathbf{T} = \mathbf{S}$, the region (Fig. 6(b)) is shrunk to form a grasping formation that holds the target object (Fig. 6(c)).

where k_l is a positive constant, and $\beta > 2$ is a constant integer so that P_i is twice differentiable. It is noted that if $\beta = 1$, then P_i is not differentiable at the boundaries of the regions where $f_l(\Delta Y_i) = 0$. Therefore, β is set to be greater than 2 so that P_i is at least twice differentiable.

A region error $\Delta\xi_i$ of the i^{th} grasping particle is defined as follows:

$$\begin{aligned}\Delta\xi_i &= \frac{\partial P_i}{\partial(\Delta Y_i)} \\ &= \sum_{l=1}^{m} k_l \left[\max(0, f_l(\Delta Y_i))\right]^{\beta-1} \left(\frac{\partial f_l(\Delta Y_i)}{\partial(\Delta Y_i)}\right)^T \end{aligned} \tag{5}$$

Note that when the grasping particles are outside of the desired region, the control force $\Delta\xi_i$ described in (5) drives the grasping particles towards the desired region. When the grasping particles are inside the desired region, then $\Delta\xi_i = 0$.

In addition, the minimum distance between grasping particles can be defined by the following inequality:

$$\begin{aligned} g_{ij}(\Delta Y_{ij}) &= r^2 - \|\Delta Y_i - \Delta Y_j\|^2 \\ &= r^2 - \left\|\mathbf{T}^{-1}\Delta y_{ij}\right\|^2 \leq 0, \end{aligned} \tag{6}$$

where $\Delta y_{ij} = y_i - y_j$ is the distance between grasping particle i and grasping particle j. Note that the minimum distance between grasping particles is time varying according to the transformation matrix $\mathbf{T}$. When the desired region scales up/down, the minimum distance also increases/decreases accordingly. Besides, r is chosen appropriately with respect to the desired region and the number of grasping particles so that the grasping particles can spread out over the desired region, as shown in Fig. 5 and Fig. 6.

A potential energy for the local objective function (6) is defined as:

$$Q_{ij} = \sum_{j \in N_i} \frac{k_{ij}}{\beta} [\max(0, g_{ij}(\Delta Y_{ij})]^{\beta}, \tag{7}$$

where k_{ij} are positive constants, and N_i is the set of

neighbors around grasping particle i.

Partial differentiating the potential energy Q_{ij} described in (7) with respect to ΔY_{ij}, we obtain:

$$\frac{\partial Q_{ij}}{\partial(\Delta Y_{ij})}=\sum_{j\in N_i} k_{ij}\underbrace{[\max\{0, g_{ij}(\Delta Y_{ij})\}]^{\beta-1}\left(\frac{\partial g_{ij}(\Delta Y_{ij})}{\partial(\Delta Y_{ij})}\right)^T}_{\Delta\overline{\rho}_{ij}}$$
$$\triangleq \Delta\rho_{ij}. \tag{8}$$

Note that $\Delta\rho_{ij}$ is a resultant force acting on the i^{th} grasping particle by its neighboring grasping particles. When the i^{th} grasping particle maintains the minimum distance from its neighboring grasping particles, i.e. $\left\|\mathbf{T}^{-1}\Delta y_{ij}\right\| \geq r$, then $\Delta\rho_{ij}=0$. The control force $\Delta\rho_{ij}$ is activated only when the distance between grasping particle i and any of its neighboring grasping particle is less than the minimum distance, i.e. $\left\|\mathbf{T}^{-1}\Delta y_{ij}\right\| < r$.

Let ε_i be defined as follows:

$$\Delta\varepsilon_i = \alpha_i\Delta\xi_i + \gamma\Delta\rho_{ij}, \tag{9}$$

where α_i and γ are positive constants. Note that when the grasping particle i is inside the desired region and the distance between grasping particle i and any of its neighboring grasping particle is greater than the minimum distance, then $\Delta\varepsilon_i = 0$. The control objective is to design $\mathbf{q_i}$ based on (1) to guarantee that $\Delta\varepsilon_i = 0$ for all i.

Eq. (1) can be rewritten as follows:

$$\dot{\mathbf{y}}_\mathbf{i} + k{\mathbf{B_b}}^{-1}\mathbf{y_i} - k{\mathbf{B_b}}^{-1}\mathbf{z} = k{\mathbf{B_b}}^{-1}\mathbf{q_i}. \tag{10}$$

Note that in the grasping stage, $\mathbf{q_i}$ varies while $\mathbf{z}$ is kept fixed. Next, a reference vector for the grasping particle i is defined as follows:

$$\dot{\mathbf{y}}_{\mathbf{ri}} = \dot{\mathbf{x}} - \mathbf{T}(\dot{\mathbf{T}}^{-1})(\mathbf{y_i} - \mathbf{x}), \tag{11}$$

where $\dot{\mathbf{T}}^{-1} = \frac{d}{dt}(\mathbf{T}^{-1})$. Then (10) can be rewritten as follows:

$$\mathbf{T}\Delta\dot{Y}_i + \dot{\mathbf{y}}_{\mathbf{ri}} + k{\mathbf{B_b}}^{-1}\mathbf{y_i} - k{\mathbf{B_b}}^{-1}\mathbf{z} = k{\mathbf{B_b}}^{-1}\mathbf{q_i}. \tag{12}$$

The formation grasping controller is introduced as follows:

$$\mathbf{q_i} = \mathbf{y_i} - \mathbf{z} + \dot{\mathbf{y}}_{\mathbf{ri}} - k_p\mathbf{T}^{-T}\Delta\varepsilon_i + \mathbf{Y}(\dot{\mathbf{y}}_{\mathbf{ri}})\widehat{\theta}_i, \tag{13}$$

where superscript $-T$ denotes the inverse transpose of a matrix. The adaptive regressor $\mathbf{Y}(\dot{\mathbf{y}}_{\mathbf{ri}})$ [35] is a diagonal matrix whose diagonal element is the entry of the reference vector $\mathbf{y_{ri}}$, i.e. $\mathbf{Y}(\dot{\mathbf{y}}_{\mathbf{ri}}) = diag\{y_{ri1}, y_{ry2}\}$, and $\widehat{\theta}_i \in \mathbb{R}^2$ is the adaptive parameter vector whose updating law is given as follows:

$$\dot{\widehat{\theta}}_i = -\mathbf{L_q}\mathbf{Y}(\dot{\mathbf{y}}_{\mathbf{ri}})\mathbf{T}^{-T}\Delta\varepsilon_i, \tag{14}$$

where $\mathbf{L_q} \in \mathbb{R}^{2\times 2}$ is a positive diagonal matrix.

Note that in (13), $\mathbf{Y}(\dot{\mathbf{y}}_{\mathbf{ri}})$ and $\widehat{\theta}_i$ are used to compensate the uncertainty caused by the unknown parameters k, $\mathbf{B_b}$. Substituting (13) into (12), we obtain the closed-loop equation:

$$\mathbf{T}\Delta\dot{Y}_i + (\mathbf{I_2} - k{\mathbf{B_b}}^{-1})\dot{\mathbf{y}}_{\mathbf{ri}}$$
$$+k_pk{\mathbf{B_b}}^{-1}\mathbf{T}^{-T}\Delta\varepsilon_i - k{\mathbf{B_b}}^{-1}\mathbf{Y}(\dot{\mathbf{y}}_{\mathbf{ri}})\widehat{\theta}_i = 0. \tag{15}$$

Now we are in the position to state the following lemma:

Lemma 1. Consider the dynamics of the grasping particles described by (1), then the grasping formation controller given by (13) and (14) guarantees the convergence of the system described by (15), that is $\Delta\varepsilon_i \to 0$ as $t \to \infty$ for $i = 1, ..., n$. This means that all the grasping particles converge to the desired region while maintaining the minimum distance between each other so that a grasping formation of trapped particles is generated around the target particle to hold it.

Proof. The details of the stability analysis are shown in the Appendix for completeness as this section mainly presents an idea of using a region control technique [33] for grasping of the microscopic particle.

Remark 1. In (13), the position of the laser beam is calculated and used as the input of the optical tweezers system. It is noted that the position-based control may lead to oscillation when implemented on a holographic optical tweezer system (HOT). In that case, the control technique described in [36] can be utilized to eliminate the oscillation caused by the position-based control with the use of the HOT.

4 Robotic control technique for manipulation of microscopic particles using grasping formation and motorized stage control

In the previous section, a grasping formation of trapped particles has been generated to hold the target particle. The laser beams are then fixed, and the target particle is manipulated to a desired position by moving the motorized stage. An illustration of the manipulation control objective is shown in Fig. 7.

In this section, the control law is presented for automated manipulation of the target particle with the consideration of the dynamic interactions between the target particle and grasping particles as well as the dynamics of the motorized stage.

When the grasping particles are in contact with the target particle, the dynamic equations of the grasping particles are now described as follows:

$$-\mathbf{B_b}\dot{\mathbf{y}}_\mathbf{i} + k\big((\mathbf{q_i} + \mathbf{z}) - \mathbf{y_i}\big) + \mathbf{f_i} = 0, \quad i = 1, 2, \ldots, n. \tag{16}$$

where $\mathbf{f_i}$ are the contact forces exerted by the target particle to the grasping particles. At this stage, the laser beams are fixed in the FOV, hence $\mathbf{q_i}$ is constant. The motorized stage is moving, and thus $\mathbf{z}$ is now a variable. The target particle is held by grasping particles as shown in Fig. 2, and thus the dynamics of the target particle can be described by the following equation:

$$\mathbf{B_c}\dot{\mathbf{x}} = -\sum_{i=1}^{n} \mathbf{f_i}, \tag{17}$$

where $\mathbf{B_c} \in \mathbb{R}^{2\text{x}2}$ denotes the damping matrix which is diagonal and positive definite. The mass of the target particle is also negligible due to the dominance of drag force in micromanipulation.

The dynamics of the motorized stage can be expressed as [27]:

$$\mathbf{M}\ddot{\mathbf{z}} + \mathbf{B}\dot{\mathbf{z}} = \mathbf{u}, \tag{18}$$

where $\mathbf{M} \in \mathbb{R}^{2\text{x}2}$ denotes the inertia matrix, $\mathbf{B} \in \mathbb{R}^{2\text{x}2}$ denotes the damping matrix, and $\mathbf{u} \in \mathbb{R}^2$ is the control input for the manipulator. Matrices $\mathbf{M}$ and $\mathbf{B}$ are diagonal and positive definite.

From (16), the dynamic equation for n grasping particles can be represented as follows:

$$\mathbf{B_B}\dot{\mathbf{y}} + \mathbf{K}\mathbf{y} - \mathbf{K}\mathbf{q} = \mathbf{K}\mathbf{A}^T\mathbf{z} + \mathbf{f}, \tag{19}$$

where $\mathbf{B_B} = diag\{\mathbf{B_b}, \cdots, \mathbf{B_b}\} \in \mathbb{R}^{2n\times 2n}$ and $\mathbf{K} = diag\{k\mathbf{I_2}, \cdots, k\mathbf{I_2}\} \in \mathbb{R}^{2n\times 2n}$ are diagonal and positive definite matrices, $\mathbf{f} = [\mathbf{f_1}^T, \cdots, \mathbf{f_n}^T]^T \in \mathbb{R}^{2n\times 1}$, $\mathbf{q} = [\mathbf{q_1}^T, \cdots, \mathbf{q_n}^T]^T \in \mathbb{R}^{2n\times 1}$, $\mathbf{y} = [\mathbf{y_1}^T, \cdots, \mathbf{y_n}^T]^T \in \mathbb{R}^{2n\times 1}$, and $\mathbf{A} = [\mathbf{I_2}, \cdots, \mathbf{I_2}] \in \mathbb{R}^{2\times 2n}$.

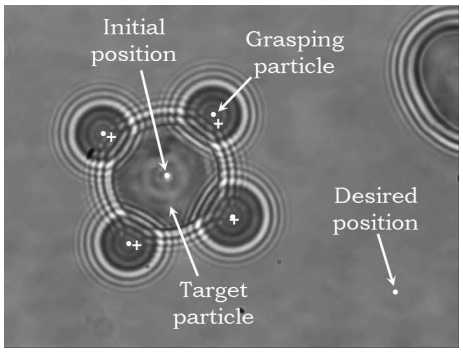

Fig. 7. Manipulation of the target particle using grasping particles and motorized stage control. The target particle is held at an initial position by trapped micro-particles, then it is manipulated to the desired position by moving the motorized stage.

The summation of the forces acting on the target particle by n grasping particles in (17) can be represented as:

$$-\sum_{i=1}^{n} \mathbf{f_i} = -\mathbf{A}\mathbf{f}. \tag{20}$$

As the grasping formation is generated to hold the target particle stably, the whole formation of grasping particles and target particle is assumed to be a rigid body. Thus the velocity of the target particle can be calculated as the average velocity of the grasping particles. If the grasping formation of the grasping particles and the target particle cannot be treated as a rigid body, then the grasping positions should be properly placed so that the position of the target particle is the average of the positions of the grasping particles, that is $\mathbf{x} = \frac{1}{n}\sum_{i=1}^{n} \mathbf{y_i}$. Thus the velocity of the target particle is described as follows:

$$\dot{\mathbf{x}} = \frac{1}{n}\sum_{i=1}^{n} \dot{\mathbf{y}}_\mathbf{i} = \frac{1}{n}\mathbf{A}\dot{\mathbf{y}}. \tag{21}$$

Multiplying both sides of (19) by $\mathbf{A}$, we obtain:

$$\mathbf{A}\mathbf{B_B}\dot{\mathbf{y}} + \mathbf{A}\mathbf{K}\mathbf{y} - \mathbf{A}\mathbf{K}\mathbf{q} = \mathbf{A}\mathbf{K}\mathbf{A}^T\mathbf{z} + \mathbf{A}\mathbf{f}. \tag{22}$$

Substituting (17), (20), and (21) into (22) we obtain the dynamic equation:

$$(\mathbf{A}\mathbf{B_B} + \frac{1}{n}\mathbf{B_c}\mathbf{A})\dot{\mathbf{y}} + \mathbf{A}\mathbf{K}\mathbf{y} - \mathbf{A}\mathbf{K}\mathbf{q} = \mathbf{A}\mathbf{K}\mathbf{A}^T\mathbf{z}. \tag{23}$$

In this control technique, the target particle is manipulated to a constant desired position $\mathbf{x_d} \in \mathbf{R}^2$ by using grasping particles and the motorized stage. The development of the controller can be resolved into two steps. First, based on the dynamic equation described in (23), a desired position input $\mathbf{z_d}$ for $\mathbf{z}$ is developed to ensure the convergence of $\mathbf{x} \to \mathbf{x_d}$. Second, based on the dynamic equation of the robotic manipulator described in (18), the control input $\mathbf{u}$ is derived using the back-stepping procedure [37] to guarantee that the actual position input $\mathbf{z}$ tracks the desired position input $\mathbf{z_d}$.

4.1 Desired Position Input for Target Particle

The aim of this subsection is to develop the desired position input $\mathbf{z_d}$ so that the position of the target particle converges to the desired position. First, we rewrite $\mathbf{z} = \mathbf{z} - \mathbf{z_d} + \mathbf{z_d} = \Delta\mathbf{z} + \mathbf{z_d}$ where $\mathbf{z_d}$ is the desired position input. Then (23) can be re-written as:

$$(\mathbf{A}\mathbf{B_B} + \frac{1}{n}\mathbf{B_c}\mathbf{A})\dot{\mathbf{y}} + \mathbf{A}\mathbf{K}\mathbf{y} - \mathbf{A}\mathbf{K}\mathbf{q}$$

$$= \mathbf{A}\mathbf{K}\mathbf{A}^T\mathbf{z_d} + \mathbf{A}\mathbf{K}\mathbf{A}^T\Delta\mathbf{z}, \tag{24}$$

where $\Delta\mathbf{z} = \mathbf{z} - \mathbf{z_d}$ represents an input pertubation. Therefore, the system in (24) can be viewed as being controlled by the fictitious input $\mathbf{z_d}$ with the pertubation $\Delta\mathbf{z}$.

Since

$$\begin{aligned}\mathbf{AK} &= (\mathbf{I_2}\cdots\mathbf{I_2})\begin{pmatrix} k\mathbf{I_2} & \dots & 0 \\ \vdots & \ddots & \vdots \\ 0 & \cdots & k\mathbf{I_2}\end{pmatrix} \\ &= (k\mathbf{I_2}\cdots k\mathbf{I_2}) = k\mathbf{A}, \end{aligned} \tag{25}$$

and

$$\begin{aligned}\mathbf{AKA}^T &= (\mathbf{I_2}\cdots\mathbf{I_2})\begin{pmatrix} k\mathbf{I_2} & \dots & 0 \\ \vdots & \ddots & \vdots \\ 0 & \cdots & k\mathbf{I_2}\end{pmatrix}(\mathbf{I_2}\cdots\mathbf{I_2})^T \\ &= nk\mathbf{I_2}, \end{aligned} \tag{26}$$

then (24) can be rewritten as:

$$(\mathbf{AB_B} + \frac{1}{n}\mathbf{B_cA})\dot{\mathbf{y}} + k\mathbf{Ay} - k\mathbf{Aq} = nk\mathbf{z_d} + nk\Delta\mathbf{z}. \tag{27}$$

The desired position input $\mathbf{z_d}$ is proposed as:

$$\mathbf{z_d} = \frac{1}{n}(\mathbf{Ay} - \mathbf{Aq}) - \mathbf{K_{px}}\Delta\mathbf{x}, \tag{28}$$

where $\Delta\mathbf{x} = \mathbf{x} - \mathbf{x_d}$ with $\mathbf{x_d} \in \mathbf{R}^2$ denoting the desired position of the target particle in stage coordinate frame $\sum_S$; $\mathbf{K_{px}} \in \mathbb{R}^{2x2}$ is a diagonal and positive definite gain matrix. Note that the relative position error of the target particle $\Delta\mathbf{x}$ in (28) can also be obtained directly in the reference frame $\sum_C$.

Substituting $\mathbf{z_d}$ into (27), we obtain the closed-loop equation:

$$(\mathbf{AB_B} + \frac{1}{n}\mathbf{B_cA})\dot{\mathbf{y}} + nk\mathbf{K_{px}}\Delta\mathbf{x} = nk\Delta\mathbf{z}. \tag{29}$$

Since

$$\begin{aligned}\mathbf{AB_B} &= (\mathbf{I_2}\cdots\mathbf{I_2})\begin{pmatrix} \mathbf{B_b} & \dots & 0 \\ \vdots & \ddots & \vdots \\ 0 & \cdots & \mathbf{B_b}\end{pmatrix} \\ &= (\mathbf{B_b}\cdots\mathbf{B_b}) = \mathbf{B_bA}, \end{aligned} \tag{30}$$

then

$$(\mathbf{AB_B} + \frac{1}{n}\mathbf{B_cA})\dot{\mathbf{y}} = (\mathbf{B_b} + \frac{1}{n}\mathbf{B_c})\mathbf{A}\dot{\mathbf{y}} = (n\mathbf{B_b} + \mathbf{B_c})\dot{\mathbf{x}}. \tag{31}$$

Substituting (31) into (29), we obtain:

$$(n\mathbf{B_b} + \mathbf{B_c})\dot{\mathbf{x}} + nk\mathbf{K_{px}}\Delta\mathbf{x} = nk\Delta\mathbf{z}. \tag{32}$$

In order to analyze the stability of the system in (32), a Lyapunov-like candidate function V_x is proposed as follows:

$$V_x = \frac{1}{2n}\Delta\mathbf{x}^T(n\mathbf{B_b} + \mathbf{B_c})\Delta\mathbf{x}, \tag{33}$$

where $(n\mathbf{B_b} + \mathbf{B_c})$ is symmetric and positive definite. Differentiating V_x with respect to time, we obtain:

$$\dot{V}_x = \frac{1}{n}\Delta\mathbf{x}^T(n\mathbf{B_b} + \mathbf{B_c})\dot{\mathbf{x}}. \tag{34}$$

Substituting (32) into (34) we obtain:

$$\dot{V}_x = -k\Delta\mathbf{x}^T\mathbf{K_{px}}\Delta\mathbf{x} + k\Delta\mathbf{x}^T\Delta\mathbf{z}. \tag{35}$$

For illustration, we first set $\Delta\mathbf{z} = \mathbf{0}$ and show the convergence of the position error $\Delta\mathbf{x} \to 0$. The control input $\mathbf{u}$ will be developed in the next subsection to ensure the convergence of both $\Delta\mathbf{z} \to 0$ and $\Delta\mathbf{x} \to 0$.

If $\Delta\mathbf{z} = \mathbf{0}$, the convergence of the position error can be stated as in the following lemma:

Lemma 2. Consider the system described by (24), if $\Delta\mathbf{z} = \mathbf{0}$, then the desired position input in (28) guarantees the convergence of $\Delta\mathbf{x} \to 0$ as $t \to \infty$.

Proof. From (33), it is clear that V_x is positive definite in $\Delta\mathbf{x}$. Since $\Delta\mathbf{z} = \mathbf{0}$, $\dot{V}_x$ is negative definite in $\Delta\mathbf{x}$. Therefore, V_x is bounded, and thus $\Delta\mathbf{x}$ is bounded. From (32), we have $\dot{\mathbf{x}}$ is bounded also. Therefore, $\Delta\mathbf{x}$ is uniformly continuous. From (33) and (35), it is clear that $\Delta\mathbf{x} \in L_2(0, +\infty)$. Therefore, we can conclude about the convergence of $\Delta\mathbf{x} \to 0$ as $t \to \infty$ by using Barbalat's lemma [38].

4.2 Control Input for Robotic Manipulator

In the previous subsection, we considered the case where $\Delta\mathbf{z} = \mathbf{0}$ to show the convergence of $\Delta\mathbf{x} \to 0$ as $t \to \infty$. Now we develop a control input $\mathbf{u}$ to ensure the convergences of both $\Delta\mathbf{z} \to \mathbf{0}$ and $\Delta\mathbf{x} \to 0$ as $t \to \infty$.

First, a sliding vector $\mathbf{s}$ using the desired position input is presented as:

$$\mathbf{s} = \dot{\mathbf{z}} - \dot{\mathbf{z}}_\mathbf{r} = \dot{\mathbf{z}} - \dot{\mathbf{z}}_\mathbf{d} + \sigma\Delta\mathbf{z}, \tag{36}$$

where $\dot{\mathbf{z}}_\mathbf{r} = \dot{\mathbf{z}}_\mathbf{d} - \sigma\Delta\mathbf{z}$ is a reference vector, and σ is a positive constant.

By using the sliding vector $\mathbf{s}$, the dynamic equation of the robotic manipulator described in (18) can be re-written as:

$$\mathbf{M}\dot{\mathbf{s}} + \mathbf{Bs} + \mathbf{Y_z}(\dot{\mathbf{z}}_\mathbf{r}, \ddot{\mathbf{z}}_\mathbf{r})\theta_z = \mathbf{u}, \tag{37}$$

where $\mathbf{Y_z}(\dot{\mathbf{z}}_\mathbf{r}, \ddot{\mathbf{z}}_\mathbf{r}) \in \mathbb{R}^{2\times p}$ is a regressor matrix, and $\theta_z \in \mathbb{R}^{p\times 1}$ is a parameter vector.

The control input $\mathbf{u}$ for the robotic manipulator is proposed as follows:

$$\mathbf{u} = -\mathbf{K_s}\mathbf{s} - \mathbf{K_z}\Delta\mathbf{z} + \mathbf{Y_z}(\dot{\mathbf{z}}_\mathbf{r}, \ddot{\mathbf{z}}_\mathbf{r})\hat{\theta}_z, \tag{38}$$

where $\mathbf{K_s} \in \mathbb{R}^{2\times 2}$ and $\mathbf{K_z} \in \mathbb{R}^{2\times 2}$ are diagonal and positive definite matrices, and $\hat{\theta}_z$ is the estimation of θ_z with the update law:

$$\dot{\hat{\theta}}_z = -\mathbf{L_z}\mathbf{Y_z}^T(\dot{\mathbf{z}}_\mathbf{r}, \ddot{\mathbf{z}}_\mathbf{r})\mathbf{s}, \tag{39}$$

where $\mathbf{L_z} \in \mathbb{R}^{p\times p}$ is a symmetric and positive definite matrix.

Substituting the control input $\mathbf{u}$ in (38) into (37), we obtain the closed-loop dynamic equation as follows:

$$\mathbf{M}\dot{\mathbf{s}} + (\mathbf{B} + \mathbf{K_s})\mathbf{s} + \mathbf{K_z}\Delta\mathbf{z} + \mathbf{Y_z}(\dot{\mathbf{z}}_\mathbf{r}, \ddot{\mathbf{z}}_\mathbf{r})\Delta\theta_z = \mathbf{0}, \tag{40}$$

where $\Delta\theta_z = \theta_z - \hat{\theta}_z$.

To analyze the stability of the overall system, a Lyapunov-like candidate function is proposed as:

$$V = V_x + V_z$$

$$= V_x + \frac{1}{2}\mathbf{s}^T\mathbf{M}\mathbf{s} + \frac{1}{2}\Delta\mathbf{z}^T\mathbf{K_z}\Delta\mathbf{z} + \frac{1}{2}\Delta\theta_z^T\mathbf{L_z}^{-1}\Delta\theta_z, \tag{41}$$

where V_x is defined in (33).

Differentiating V with respect to time, we obtain:

$$\dot{V} = \dot{V}_x + \dot{V}_z = \dot{V}_x + \mathbf{s}^T\mathbf{M}\dot{\mathbf{s}} + \Delta\mathbf{z}^T\mathbf{K_z}\Delta\dot{\mathbf{z}} - \dot{\hat{\theta}}_z^T\mathbf{L_z}^{-1}\Delta\theta_z. \tag{42}$$

Substituting (39) and (40) into (42), and using (35), we obtain:

$$\dot{V} = \dot{V}_x - \mathbf{s}^T(\mathbf{B}+\mathbf{K_s})\mathbf{s} - (\Delta\dot{\mathbf{z}}+\sigma\Delta\mathbf{z})^T\mathbf{K_z}\Delta\mathbf{z} + \Delta\mathbf{z}^T\mathbf{K_z}\Delta\dot{\mathbf{z}}$$

$$= -k\Delta\mathbf{x}^T\mathbf{K_{px}}\Delta\mathbf{x} + k\Delta\mathbf{x}^T\Delta\mathbf{z} - \mathbf{s}^T(\mathbf{B}+\mathbf{K_s})\mathbf{s} - \sigma\Delta\mathbf{z}^T\mathbf{K_z}\Delta\mathbf{z}$$

$$= -\mathbf{s}^T(\mathbf{B}+\mathbf{K_s})\mathbf{s}$$

$$-(\Delta\mathbf{z}^T\ \Delta\mathbf{x}^T)\begin{pmatrix} \sigma\mathbf{K_z} & -\frac{1}{2}k\mathbf{I_2} \\ -\frac{1}{2}k\mathbf{I_2} & k\mathbf{K_{px}} \end{pmatrix}(\Delta\mathbf{z}^T\ \Delta\mathbf{x}^T)^T. \tag{43}$$

Let the controller parameters σ and $\mathbf{K_z}$, $\mathbf{K_{px}}$ be chosen such that

$$\sigma\lambda_{min}[\mathbf{K_z}\mathbf{K_{px}}] > \frac{1}{4}k, \tag{44}$$

then $\mathbf{Q} = \begin{pmatrix} \sigma\mathbf{K_z} & -\frac{1}{2}k\mathbf{I_2} \\ -\frac{1}{2}k\mathbf{I_2} & k\mathbf{K_{px}} \end{pmatrix}$ is positive definite, with $\lambda_{min}[\cdot]$ denoting the minimum eigenvalue of the matrix. We can now state the following theorem:

Theorem. Consider the optical tweezers system described by (16), (17), (18), then the control input for the robotic manipulator given by (38), (39), and (28) with the control gains chosen as in (44) guarantees the convergence of the closed-loop system so that $\Delta\mathbf{x} \to 0$ and $\Delta\mathbf{z} \to 0$ as $t \to \infty$.

Proof. From (33) and (41), it is clear that V is positive definite in $\Delta\mathbf{x}$, s, $\Delta\mathbf{z}$, and $\Delta\theta_z$. With the controller parameters satisfy (44), $\dot{V}$ is negative definite in s, $\Delta\mathbf{z}$ and $\Delta\mathbf{x}$. Therefore, V is bounded, and thus $\Delta\mathbf{x}$, $\mathbf{s}$, $\Delta\mathbf{z}$ and $\Delta\theta_z$ are bounded. From (36), the boundedness of $\mathbf{s}$ and $\Delta\mathbf{z}$ guarantees the boundedness of $\Delta\dot{\mathbf{z}}$. Therefore, $\Delta\mathbf{z}$ is uniformly continuous. Since $\Delta\mathbf{z}$ and $\Delta\mathbf{x}$ are bounded, then $\dot{\mathbf{x}}$ is bounded from (32). Therefore, $\Delta\mathbf{x}$ is uniformly continuous. From (33), (41) and (43), it is clear that $\Delta\mathbf{z}, \Delta\mathbf{x} \in L_2(0, +\infty)$. Then it follows that $\Delta\mathbf{z} \to \mathbf{0}$ and $\Delta\mathbf{x} \to 0$ as $t \to \infty$ by using Barbalat's lemma [38].

Remark 2. The overall dynamics of the robotic manipulator interacting with the grasping particles and the target particle described in (16), (17), and (18) has third-order dynamics. In order to avoid the use of the high-order derivatives due to the third-order dynamics, adaptive observers [39] can be used.

5 Experiment

The proposed control technique was implemented in the optical tweezers system as shown in Fig. 8. The system consists of a multiple optical trap device (Elliot Scientific, E3500), a motorized stage (Marzhauser Wetzlar, SCAN IM), an inverted microscope (Nikon, Eclipse Ti-U), and a digital camera (Basler, pi640-210gm). The operation of the motorized stage is in 2-D space, with the range of $120mm \times 100mm$ and the resolution of $0.01\mu m$. The FOV of the camera is a rectangle with the dimensions of $47.95\mu m \times 36.11\mu m$. By utilizing acousto optic deflectors (AODs), the optical tweezers system is able to create and manipulate multiple laser beams within the FOV with the resolution of $16\rho m$. The position of the laser beams can be measured by using either the camera or encoders mounted on the stage, while the position of

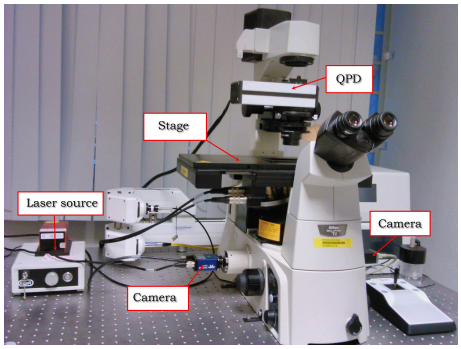

Fig. 8. Optical tweezers system consists of a microscope, a motorized stage, an optical trap device, and two cameras.

the micro-particles are measured by using the camera. The control methodology has been programmed in National Instruments LabVIEW that could simultaneously control the motorized stage and the laser traps.

To illustrate the performance of the proposed controller, four $5\mu m$ diameter latex micro-beads (with the density of $1500kg/m^3$, and a refractive index of 1.60) were trapped and driven to a desired region around a target particle, which is specified as follows:

$$\begin{aligned} f_1(\Delta Y_i) &= R_1^2 - \{\Delta Y_{i1}\}^2 - \{\Delta Y_{i2}\}^2 \leq 0 \\ f_2(\Delta Y_i) &= \{\Delta Y_{i1}\}^2 + \{\Delta Y_{i2}\}^2 - R_2^2 \leq 0. \end{aligned} \tag{45}$$

By using a transformation matrix, the desired region was first scaled down to form a grasping formation to hold the target particle. After the target particle was held, it was also rotated around its center. The target particle was then manipulated to a desired position by using the motorized stage. In this experiment, a cornflour particle with approximate diameter of $8\mu m$ was used as the target particle. Since the cornflour particle is inert due to its large size, it was difficult to directly trap and manipulate it using a single laser beam.
(i) First, four laser beams were generated, and each laser beam trapped a $5\mu m$ micro-bead as shown in Fig. 9(a). Then the trapped micro-particles are automatically driven to the desired region (45). By using the transformation matrix

$$\mathbf{T} = \mathbf{SR} = \begin{bmatrix} s_x(t) & 0 \\ 0 & s_y(t) \end{bmatrix} \begin{bmatrix} \cos\phi(t) & \sin\phi(t) \\ -\sin\phi(t) & \cos\phi(t) \end{bmatrix}, \tag{46}$$

with

$$s_x(t) = s_y(t) = \begin{cases} \frac{3}{2} - \frac{1}{2}\left[-3\left(\frac{t}{t_1}\right)^4 + 4\left(\frac{t}{t_1}\right)^3\right], & t < t_1 \\ 1, & t \geq t_1 \end{cases} \tag{47}$$

and

$$\phi(t) = \begin{cases} 0, & t < t_1 \\ \phi_1\left[-3\left(\frac{t-t_1}{t_2-t_1}\right)^4 + 4\left(\frac{t-t_1}{t_2-t_1}\right)^3\right], & t_1 \leq t < t_2 \\ \phi_1, & t \geq t_2 \end{cases} \tag{48}$$

the desired region was first scaled down ($t < t_1$) until the grasping formation was achieved. Then the target particle was rotated by an angle ϕ_1 around its center for $t_1 \leq t < t_2$. It is noted that the different time points t_1, t_2 are user-defined. These parameters are specified according to the desired rotational speed of the grasping formation. The power of the laser source was set at $0.2W$, and the control parameters were set as $\mathbf{L_q} = 10^{-5} \times \mathbf{I_2}$, $k_p = 5 \times 10^{-4}$, with $\phi_1 = -4\pi/9$, $t_1 = 2s, t_2 = 8s$, and $\gamma = \alpha_i = 1$ for $i = 1, 2, ..., n$. The snapshots of the scaling formation at different time instants are shown in Fig. 9, and the snapshots of rotated formation are shown in Fig. 10.

(ii) Next, the laser beams were fixed to hold the cornflour particle in the medium. The cornflour particle was then manipulated to a desired position by moving the motorized stage. Finally, the trapped micro-particles were released from the grasping formation. The control parameters were set as $n = 4$, $\mathbf{K_{px}} = 0.02 \times \mathbf{I_2}$, $\sigma = 1$, $\mathbf{K_s} = \mathbf{I_2}, \mathbf{K_z} = \mathbf{I_2}, \mathbf{L_z} = 10^{-5} \times \mathbf{I_4}$. The initial position of the cornflour particle was $(17.67\mu m, -18.72\mu m)^T$, and then it was manipulated to the desired position $\mathbf{x_d} = (41.74\mu m, -34.78\mu m)^T$, both positions are defined with respect to the stage coordinate frame $\sum_S$. The snapshots of manipulation at different time instants are shown in Fig. 11. The errors between the position of the cornflour particle and its desired position during transportation are shown Fig. 12. The target particle was transported to the desired position in approximately 6 seconds.

In the second experiment, three $5\mu m$ micro-beads were utilized to grasp and manipulate another target object, as shown in Fig. 13(a). The target object is also a cornflour particle but with a bell-like shape. By using the transformation matrix $\mathbf{T}$ (46) where

$$\phi(t) = \begin{cases} 0, & t < t_1 \\ \phi_2\left[-3\left(\frac{t-t_1}{t_2-t_1}\right)^4 + 4\left(\frac{t-t_1}{t_2-t_1}\right)^3\right], & t_1 \leq t < t_2 \\ \phi_2, & t_2 \leq t < t_3 \\ \phi_2 - \frac{\pi}{2}\left[-3\left(\frac{t-t_3}{t_4-t_3}\right)^4 + 4\left(\frac{t-t_3}{t_4-t_3}\right)^3\right], & t_3 \leq t < t_4 \\ \phi_2 - \frac{\pi}{2}, & t \geq t_4 \end{cases} \tag{49}$$

and

$$s_x(t) = s_y(t) = \begin{cases} \frac{15}{4}, & t < t_2 \\ \frac{15}{4} - \frac{11}{4}\left[-3\left(\frac{t-t_2}{t_3-t_2}\right)^4 + 4\left(\frac{t-t_2}{t_3-t_2}\right)^3\right], & t_2 \leq t < t_3 \\ 1, & t \geq t_3 \end{cases} \tag{50}$$

the grasping particles were first driven to a desired region (Fig. 13(b)). In order to achieve appropriate grasping points, the grasping particles were rotated around the target object by an angle $\phi_2 = -\pi/3$ for $t_1 \leq t < t_2$. Then the desired region was scaled down ($t_2 \leq t < t_3$) to form a grasping formation to hold the target particle, as shown in Fig. 13(f). Next, the target particle was rotated by another angle $-\pi/2$ by rotating the grasping formation for $t_3 \leq t < t_4$. Finally, the target particle was manipulated to a desired position by motorized stage control, as shown in Fig. 13(k). The control parameters

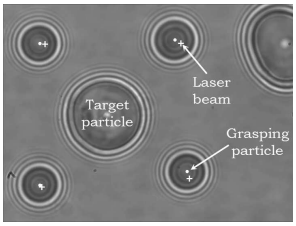

(a) Beginning of grasping stage at $t = 0s$. Four micro-particles are trapped by four laser beams.

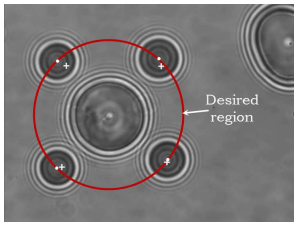

(b) $t = 1s$. The trapped micro-particles are driven to the region.

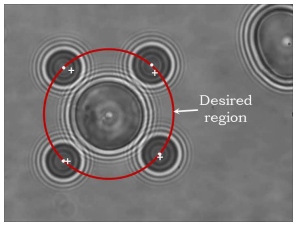

(c) $t = 1.5s$. The region is scaled down.

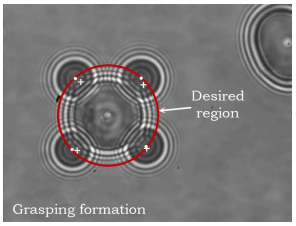

(d) $t = 2s$. The grasping formation is generated to hold the target cell.

Fig. 9. The grasping of the target particle using grasping particles and a scaling region. By using the scaling transformation matrix, the desired region was shrunk to form the grasping formation to hold the target particle. The "+" denotes the laser beam position, and the "·" denotes the position of the micro-particle.

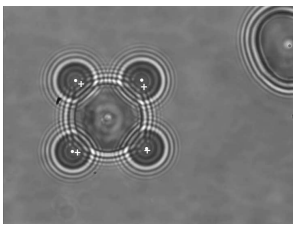

(a) t=2s

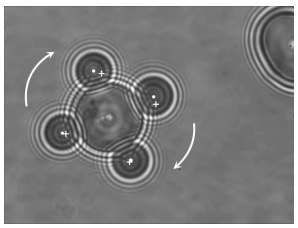

(b) t=4s

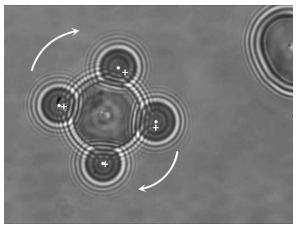

(c) t=6s

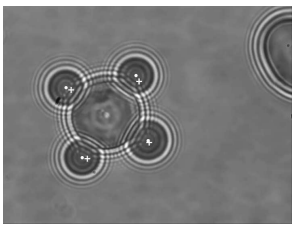

(d) t=8s

Fig. 10. Snapshots of the rotational motion of the system at different time instants. By using rotational transformation matrix, the trapped micro-particles are rotated which lead to the rotation of the target particle around its initial position.

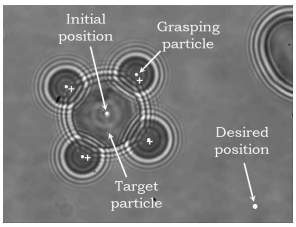

(a) Beginning of manipulation stage at $t_t = 0s$.

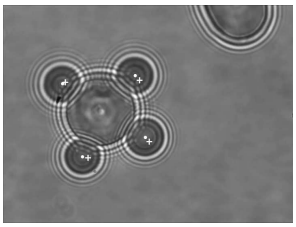

(b) $t_t = 2s$.

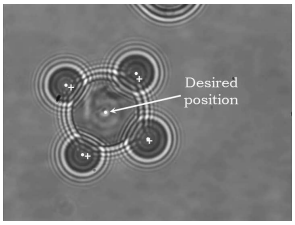

(c) $t_t = 6s$. The target particle is at the desired position.

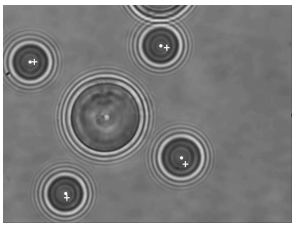

(d) $t_t = 9s$. The target particle is released from the grasping formation.

Fig. 11. Manipulation of the target particle using trapped micro-particles and motorized stage control. The cornflour particle is manipulated to the desired position by moving the motorized stage while fixing the laser beams in the FOV to suspend the cornflour particle in the medium.

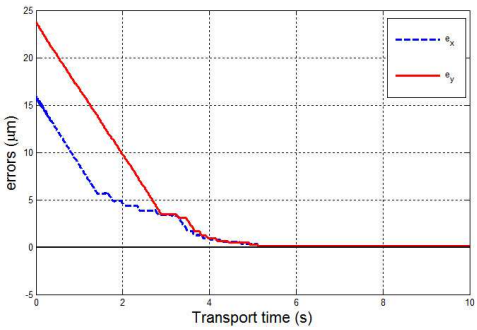

Fig. 12. The errors between the position of the cornflour particle and its desired position.

were set as in the previous experiment, with $t_1 = 2s$, $t_2 = 5s$, $t_3 = 8s$, and $t_4 = 14s$. The initial position of the target particle was $(22.10\mu m, -14.89\mu m)^T$, and then it was manipulated to the desired position $\mathbf{x_d} = (41.74\mu m, -34.78\mu m)^T$, both positions are defined with respect to the stage coordinate frame $\sum_S$. The snapshots of grasping and manipulation of the target particle at different time instants are shown in Fig. 13. The errors between the position of the target particle and its desired position during transportation are shown in Fig. 14.

Remark 3. If the speed of the motorized stage is too high, then the grasping formation may lose balance and finally lead to a failed manipulation task. To avoid this problem, a saturated controller [40] can be implemented

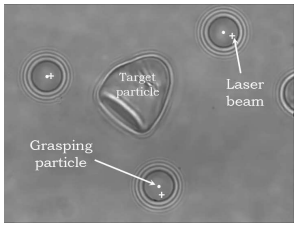

(a) Beginning of grasping stage at $t = 0s$. The grasping particles are trapped and brought around the target object

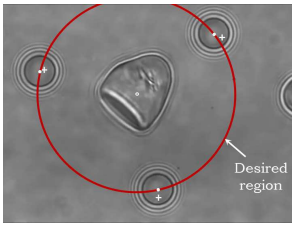

(b) $t = 2s$. The grasping particles are driven to a desired region centred around the target object

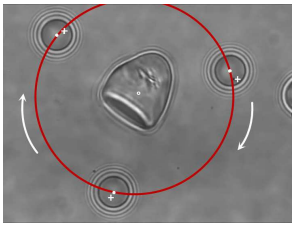

(c) $t = 3s$. The region is being rotated.

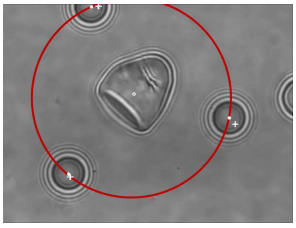

(d) $t = 5s$. The region stops rotating and starts scaling.

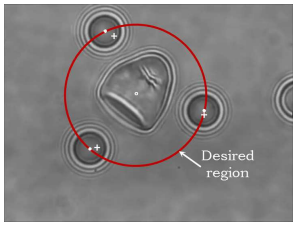

(e) $t = 6s$. The region is being scaled down.

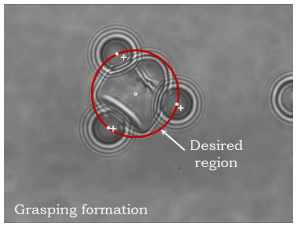

(f) $t = 8s$. A grasping formation is generated to hold the target particle

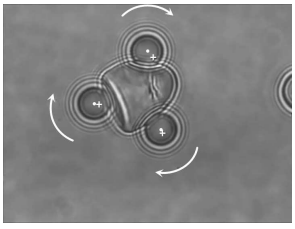

(g) $t = 11s$. The target particle is being rotated by rotating the grasping formation.

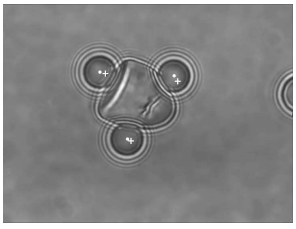

(h) $t = 14s$. The region stops rotating.

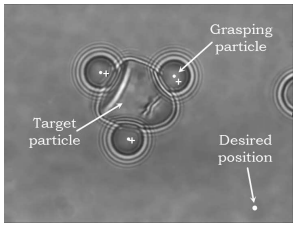

(i) Beginning of manipulation stage at $t_t = 0s$. The laser beams are fixed, and the target particle is manipulated to the desired positon by controlling the motorized stage.

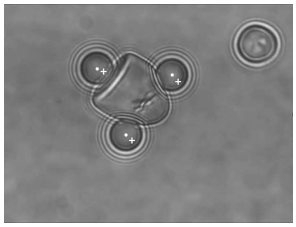

(j) $t_t = 2s$.

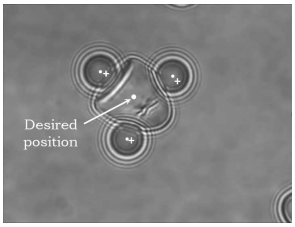

(k) $t_t = 5s$. The target particle is at the desired position.

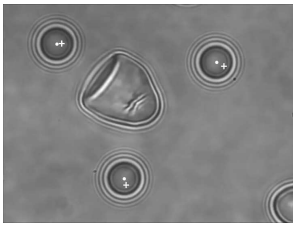

(ℓ) $t_t = 8s$. The target particle is released from the grasping formation.

Fig. 13. Experiment 2: Grasping and manipulation of a bell-like target particle.

to restrain the speed of the motorized stage movement.

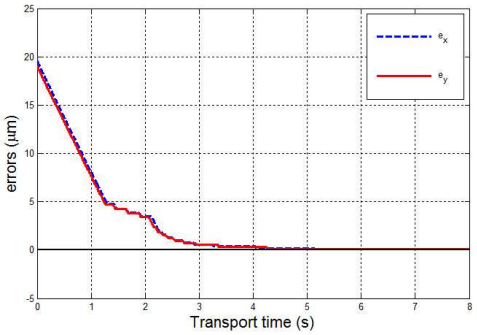

Fig. 14. Experiment 2: The errors between the position of the cornflour particle and its desired position.

6 Conclusion

In this paper, robotic control techniques have been presented to achieve grasping and manipulation of a microscopic particle. A grasping formation of trapped particles is first generated to hold the target particle in the medium, and motorized stage control is then used to manipulate the target particle to the desired position. The proposed strategy is particularly suitable for manipulation of various types of microscopic particles, including laser-sensitive biological cells, large particles, or even particles which cannot be directly trapped and manipulated by using only one single optical trap. Rigorous mathematical formulations have been developed to analyze the control system, with the consideration of the dynamic interactions between the target particle and the grasping particles as well as the dynamics of the motor-

ized stage, which acts as a robotic manipulator. Experimental results have been presented to illustrate the performance of the proposed techniques. This paper considers the grasping and manipulation of the target particle in a two-dimensional workspace. Future work would be devoted to implementing the proposed control techniques on a three-dimensional motorized stage. That is, after the target particle has been grasped by the grasping particles, the motorized stage is moved in three dimensions to perform the manipulation tasks.

Acknowledgements

This work was supported by the Agency For Science, Technology And Research of Singapore (A*STAR), (Reference No. 1121202014).

References

[1] Kreplak, L., Wang, H., Aebi, U., & Kong, X. P. (2007). Atomic force microscopy of mammalian urothelial surface. *Journal of Molecular Biology*, 374(2), 365-373.

[2] Kasaya, T., Miyazaki, H. T., Saito, S., & Sato, T. (1999). Micro object handling under SEM by vision-based automatic control. *IEEE International Conference on Robotics and Automation*, 2189-2196.

[3] Zhang, Y., Chen, B. K., Liu, X., & Sun, Y. (2010). Autonomous robotic pick and place of micro-objects. *IEEE Transactions on Robotics*, 26(1), 200-207.

[4] Pawashe, C., Floyd, S., & Sitti, M. (2009). Modeling and experimental characterization of an untethered magnetic micro-robot. *International Journal of Robotics Research*, 28(8), 1077-1094.

[5] Zhang, Z., Huang, Y., & Menq, C. H. (2010). Visually controlled manipulation of a magnetic microbead using magnetic tweezers. *IEEE Transactions on Robotics*, 26(3), 531-541.

[6] Yesin, K.B., Vollmers, K., & Nelson, B. J. (2006). Modeling and control of untethered biomicrorobots in a fluidic environment using electromagnetic fields. *International Journal of Robotics Research*, 25(4-5), 527-536.

[7] Curtis, J. E., Koss, B. A., & Grier, D. G. (2002). Dynamic holographic optical tweezers. *Optics Communications*, 207, 169-175.

[8] Ashkin, A. (1970). Acceleration and trapping of particles by radiation pressure. *Physical Review Letters*, 24, 156-159.

[9] Ashkin, A., Dziedzic, J. M., Bjorkholm, J. E., & Chu, S. (1986). Observation of a single-beam gradient force optical trap for dielectric particles. *Optical Letters*, 11(5), 288-290.

[10] Ashkin, A. (2000). History of optical trapping and manipulation of small- neural particle, atoms, and molecules. *IEEE Journal on Selected Topics in Quantum Electronics*, 6(6), 841-856.

[11] Murata, M., Okamoto, Y., Park, Y., Kaji, N., Tokeshi, M., & Baba, Y. (2009). Cell separation by the combination of microfluidics and optical trapping force on a microchip. *Analytical and Bioanalytical Chemistry*, 394, 277-283.

[12] Rusu, C., Oever, R., Boer, M. J., Jansen, H. V., Berenschot, J. W., Bennink, M. L., Kanger, J. S., Grooth, B. G., Elwenspoek, M., Greve, J., Brugger, J., & Berg, A. (2001). Direct integration of micomachined pipettes in a flow channel for single DNA molecule study by optical tweezers. *Journal of Microelectromechanical Systems*, 10(2), 238-245.

[13] Tan, Y., Sun, D., Wang, J., & Huang, W. (2010). Mechanical characterization of human red blood cells under different osmotic conditions by robotic manipualtion with optical tweezers. *Transactions on Biomedical Engineering*, 57(7), 1816-1825.

[14] Vermeulena, K. C., Mamerena, J. V., Stienen, G. J. M., Peterman, E. J. G., Wuite, G. J. L., & Schmidt, C. F. (2006). Calibrating bead displacements in optical tweezers using acousto-optic deflectors. *Review of Scientific Instruments*, 77, 013704.

[15] Visscher, K., Brakenhoff, G. J., & Kroll, J. J. (1993). Micromanipulation by multiple optical traps created by a single fast scanning trap integrated with the bilateral confocal scanning laser microscope. *Cytometry*, 14, 105-114.

[16] Arai, F., Yoshikawa, K., Sakami, T., & Fukuda, T. (2004). Synchronized laser micromanipulation of multiple targets along each trajectory by single laser. *Applied Physics Letters*, 85, 4301-4304.

[17] Dufresne, E., Spalding, G., Dearing, M., Sheets, S., & Grier, D. (2001). Computer-generated holographic optical tweezers arrays. *Review of Scientific Instruments*, 72, 1810-1816.

[18] Leach, J., Sinclair, G., Jordan, P., Courtial, M. J. P. J., Cooper, J., & Laczik, Z. J. (2004). 3D manipulation of particles into crystal structures using holographic optical tweezers. *Optics Express*, 12, 220-226.

[19] MacDonald, M., Spalding, G., & Dholakia, K. (2003). Microfluidic sorting in an optical lattice. *Nature*, 426, 421-424.

[20] Chowdhury, S., Svec, P., Wang, C., Losert, W., & Gupta, S. K. (2012). Gripper synthesis for indirect manipulation of cells using holographic optical tweezers. *IEEE International Conference on Robotics and Automation*, 2749-2754.

[21] Chowdhury, S., Thakur, A., Wang, C., Svec, P., Losert, W., & Gupta, S. K. (2014). Automated manipulation of biological cells using gripper formations controlled by optical tweezers. *IEEE Transactions on Automation Science and Engineering*, 11, 338-347.

[22] Ibanez, C. A., Castanon, M. S. S., & Soriano, R. (2011). A simple control scheme for the manipulation of a particle by means of optical tweezers. *International Journal of Robust and Nonlinear Control*, 21, 328-337.

[23] Hu, S., & Sun, D. (2011). Transportation of biological cells with robot-tweezer manipulation system. *IEEE International Conference on Robotics and Automation*, Shanghai, 5997-6002.

[24] Ranaweeraz, A., & Bamieh, B. (2005). Modelling, identication, and control of a spherical particle trapped in an optical tweezer. *International Journal of Robust and Nonlinear Control*, 15, 747-768.

[25] Tanaka, Y., Kawada, H., Hirano, K., Ishikawa, M., & Kitajima, H. (2008). Automated manipulation of non-spherical micro-objects using optical tweezers combined with image processing techniques. *Optics Express*, 16(19), 15115-15122.

[26] Li, X., & Cheah, C. C. (2012). Dynamic region control for robot-assisted cell manipulation using optical tweezers. *IEEE International Conference on Robotics and Automation*, Minesota, USA, 1057-1062.

[27] Li, X., Cheah, C. C., Hu, S., & Sun, D. (2013). Dynamic trapping and manipulation of biological cells with optical tweezers. *Automatica*, 49, 1614-1625.

[28] Yan, X., Cheah, C. C., Pham, Q. C., & Slotine, J. J. E. (2015). Robotic manipulation using optical tweezers with velocity constraints and stochastic perturbations", IEEE International Conference on Robotics and Automation, Washington, USA.

[29] Chen, H., & Sun, D. (2012). Moving groups of microparticles into array with a robottweezers manipulation system. *IEEE Transactions on Robotics*, 28(5), 1069-1080.

[30] Chen, H., & Lou, Y. (2013). Flocking multiple microparticles with automatically controlled optical tweezers: solutions and experiments. *IEEE Transactions on Biomedical Engineering*, 60, 1518-1527.

[31] Haghighi, R., & Cheah, C. C. (2015). Optical micromanipulation of multiple groups of cells. *IEEE International Conference on Robotics and Automation*, Washington, USA, 3543-3548. (an extended version was submitted to IEEE Transactions on Robotics)

[32] Cheah, C. C., Ta, Q. M., & Haghighi, R. (2015). Robotic manipulation of a biological cell using multiple optical traps. *IEEE International Conference on Robotics and Automation*, Washington, USA, 803-808.

[33] Cheah, C. C., Hou, S. P., & Slotine, J. J. E. (2009). Region-based shape control for a swarm of robots. *Automatica*, 45, 2406-2411.

[34] Reuleaux, F. (1876). The kinematics of machinery, *A. B. Kennedy, Ed. New York, NY, USA: Macmillan and Co.*.

[35] Slotine, J. E., & Li, W. (1987). On the adaptive control of robot manipulators. *The International Journal of Robotics Research*, 6(3), 49-59.

[36] Chen, H., & Sun, D. (2015). Swarm-Inspired Transportation of Biological Cells Using Saturation-Controlled Optical Tweezers, *IEEE International Conference on Robotics and Automation*, Washington, USA, 3531-3536.

[37] Kokotovic, P. V. (1992). The joy of feedback: nonlinear and adaptive. *IEEE Control Systems Magazine*, 12(3), 7-17.

[38] Slotine, J. E., & Li, W. (1991). Applied nonlinear control. *Prentice Hall*.

[39] Cheah, C. C., Li, X., Yan, X., & Sun, D. (2014). Observer based optical manipulation of biological cells with robotic tweezers. *IEEE Transactions on Robotics*, 30(1), 68-80.

[40] Arimoto, S. (1996). Control theory of nonlinear mechanical systems - A passivity-based and circuit-theoretic approach. *Oxford: Clarendon Press*.

A Appendix

In this appendix, we present the proof of lemma 1 stated in Section 3:

Proof : The second term of (15) can be expressed as follows

$$(\mathbf{I_2} - k{\mathbf{B_b}}^{-1})\dot{\mathbf{y}}_{\mathbf{ri}} = diag\{\dot{y}_{ri1}, \dot{y}_{ri2}\}(1 - \frac{k}{b_{b1}}, 1 - \frac{k}{b_{b2}})^T = \mathbf{Y}(\dot{\mathbf{y}}_{\mathbf{ri}})\chi, \quad (A.1)$$

where $\chi = (1 - k/b_{b1}, 1 - k/b_{b2})^T$ is unknown.

Substituting (A.1) into (15), we obtain:

$$\mathbf{T}\Delta\dot{Y}_i + \mathbf{Y}(\dot{\mathbf{y}}_{\mathbf{ri}})(\chi - k{\mathbf{B_b}}^{-1}\widehat{\theta}_i) + k_p k{\mathbf{B_b}}^{-1}{\mathbf{T}}^{-T}\Delta\varepsilon_i = 0. \quad (A.2)$$

The Lyapunov-like candidate function is introduced as follows:

$$V_q = \sum_{i=1}^{n}\alpha_i P_i + \frac{1}{2}\sum_{i=1}^{n}\gamma Q_{ij} + \sum_{i=1}^{n}\frac{1}{2}(k^{-1}\mathbf{B_b}\chi - \widehat{\theta}_i)^T{\mathbf{L_q}}^{-1}k{\mathbf{B_b}}^{-1}(k^{-1}\mathbf{B_b}\chi - \widehat{\theta}_i), \quad (A.3)$$

where ${\mathbf{L_q}}^{-1}k{\mathbf{B_b}}^{-1}$ is a positive diagonal matrix.

Taking the time-derivative of V_q, we obtain:

$$\dot{V}_q = \sum_{i=1}^{n}\alpha_i\sum_{l=1}^{m}k_l\left[\max(0, {f_l}^{\beta-1}(\Delta Y_i)\right]\Delta\dot{Y}_i^T\left(\frac{\partial f_l(\Delta Y_i)}{\partial(\Delta Y_i)}\right)^T + \frac{1}{2}\sum_{i=1}^{n}\gamma\sum_{j\in N_i}k_{ij}\Delta\dot{Y}_{ij}^T\Delta\overline{\rho}_{ij} - \sum_{i=1}^{n}\dot{\widehat{\theta}}_i^T{\mathbf{L_q}}^{-1}(\chi - k{\mathbf{B_b}}^{-1}\widehat{\theta}_i), \quad (A.4)$$

where $\Delta\overline{\rho}_{ij}$ is defined in (8). Using (6), the second term of (A.4) can be rewritten as:

$$\begin{aligned}&\frac{1}{2}\sum_{i=1}^{n}\gamma\sum_{j\in N_i}k_{ij}\Delta\dot{Y}_{ij}^T\Delta\overline{\rho}_{ij}\\ &= \frac{1}{2}\sum_{i=1}^{n}\gamma\Delta\dot{Y}_i^T\Delta\rho_{ij} + \frac{1}{2}\sum_{j=1}^{n}\gamma\sum_{i\in N_j}k_{ij}\Delta\dot{Y}_j^T\Delta\overline{\rho}_{ji}\\ &= \sum_{i=1}^{n}\gamma\Delta\dot{Y}_i^T\Delta\rho_{ij}. \end{aligned} \quad (A.5)$$

Substituting (A.2) and (A.5) into (A.4), we obtain:

$$\begin{aligned}\dot{V}_q &= \sum_{i=1}^{n}\Delta\dot{Y}_i^T\Delta\varepsilon_i - \sum_{i=1}^{n}\dot{\widehat{\theta}}_i^T{\mathbf{L_q}}^{-1}(\chi - k{\mathbf{B_b}}^{-1}\widehat{\theta}_i)\\ &= -\sum_{i=1}^{n}\{\mathbf{T}^{-1}\mathbf{Y}(\dot{\mathbf{y}}_{\mathbf{ri}})(\chi - k{\mathbf{B_b}}^{-1}\widehat{\theta}_i)\}^T\Delta\varepsilon_i\\ &\quad -kk_p\sum_{i=1}^{n}\Delta\varepsilon_i^T\mathbf{T}^{-1}{\mathbf{B_b}}^{-1}{\mathbf{T}}^{-T}\Delta\varepsilon_i\\ &\quad -\sum_{i=1}^{n}(\chi - k{\mathbf{B_b}}^{-1}\widehat{\theta}_i)^T{\mathbf{L_q}}^{-1}\dot{\widehat{\theta}}_i\\ &= -kk_p\sum_{i=1}^{n}\Delta\varepsilon_i^T\mathbf{T}^{-1}{\mathbf{B_b}}^{-1}{\mathbf{T}}^{-T}\Delta\varepsilon_i. \end{aligned} \quad (A.6)$$

From (A.3), and (A.6), V_q is non-negative and $\dot{V}_q$ is negative definite in $\Delta\varepsilon_i$, hence V_q is bounded. Therefore,

P_i and Q_{ij} are bounded. From (4) and (7), $f_l(\Delta Y_i)$ and $g_{ij}(\Delta Y_{ij})$ are bounded. Therefore $\mathbf{y_i}$ is bounded if $\mathbf{x}$ is bounded. Hence, $\frac{\partial f_l(\Delta Y_i)}{\partial(\Delta Y_i)}$ and $\frac{\partial g_{ij}(\Delta Y_{ij})}{\partial(\Delta Y_{ij})}$ are bounded. From (9), $\Delta\varepsilon_i$ is bounded.

From (11), $\dot{\mathbf{y}}_{\mathbf{ri}}$ is bounded if $\dot{\mathbf{x}}$ is bounded. From (14), $\widehat{\theta}_i$ is bounded. Therefore, from (15), $\Delta\dot{Y}_i$ is bounded. Hence, from (4), and (7), $\Delta\dot{\xi}_i$ and $\Delta\dot{\rho}_{ij}$ are bounded. Therefore, $\Delta\dot{\varepsilon}_i$ is bounded. Hence, $\ddot{V}_q$ is bounded since both $\Delta\varepsilon_i$ and $\Delta\dot{\varepsilon}_i$ are bounded. Therefore, $\dot{V}_q$ is uniformly continuous. Applying Barbalat's lemma [38], we have $\dot{V}_q \to 0$ which also indicates that $\Delta\varepsilon_i \to 0$ as $t \to \infty$ for $i = 1, ..., n$.